

Article

Experimental Setup of the Fast Current Controller for the Buenos Aires Heavy Ion Microbeam

Nahuel Agustín Vega ^{1,2,3,*}, Nahuel Agustín Müller ¹, Emmanuel de la Fourniére ^{1,2},
Emilia Beatriz Halac ^{1,2} and Mario Ernesto Debray ^{1,2}

¹ Gerencia de Investigación y Aplicaciones, CNEA, Av Gral Paz 1499, San Martín, B1650HMQ Buenos Aires, Argentina; nahuelam.93@gmail.com (N.A.M.); edlf@tandar.cnea.gov.ar (E.d.l.F.); halac@cnea.gov.ar (E.B.H.); debray@tandar.cnea.gov.ar (M.E.D.)

² Escuela de Ciencia y Tecnología, Universidad Nacional de San Martín (UNSAM), San Martín, B1650HMQ Buenos Aires, Argentina

³ Consejo Nacional de Investigaciones Científicas y Tecnológicas (CONICET), Rivadavia 1917, C1033AAJ Ciudad de Buenos Aires, Argentina

* Correspondence: nvega@tandar.cnea.gov.ar; Tel.: +54-911-6772-7067

Received: 9 April 2019; Accepted: 27 May 2019; Published: 3 June 2019



Abstract: Recently we used the heavy ion microprobe of the Buenos Aires TANDAR Laboratory for Single Event Effects (SEE) and Total Dose (TD) experiments in electronics devices and components, requiring very low beam currents. The facility includes a fast beam switch that allows the control of the ion beam current and a mobile Si PIN (p-type, intrinsic, n-type) diode that directly measures the number of ions hitting the device. The fast beam deflector was used to reduce the current by producing a pulsed beam or generating a quasi-continuous (Poisson-like distributed) beam with currents ranging from tens to hundreds of ions/s. As an application for this current control method we present a single event effect (SEE) pulses map generated by a $^{32}\text{S}^{8+}$ beam at 75 MeV on two 0.5 μm technology CMOS digital output buffers where the device was formed by cascading four CMOS inverters with increasing sizes from input to output to drive large loads. Using the same concept of pulse width modulated deflection, we developed a novel gradient scanning method. This system allows to produce in a single irradiation a distribution with a cumulative damage with a difference of two orders of magnitude at constant gradient. To demonstrate the method, we irradiated a lithium niobate monocrystal with $^{32}\text{S}^{8+}$ beam at 75 MeV energy and later analyzed the produced damage by the micro-Raman technique and an optical profilometer.

Keywords: particle beam attenuator; electrostatic deflector; ion microbeam

1. Introduction

The Buenos Aires heavy ion nuclear microprobe facility MiP (Microhaz de iones Pesados) has been in operation for fourteen years. It is one of the experimental lines of the Tandar 20UD Pelletron accelerator and comprises Oxford Microbeams Ltd. (Oxfordshire, UK) OM55 triplet of magnetic quadrupoles. It was originally set up for micro-PIXE (micro-particle induced X-Ray emission) [1–3] elemental analysis and micromachining [4,5]. Recently, it was employed in SEE (single event effects) testing, IBIC/TRIBIC (ion beam induced charge/time-resolved IBIC) measurements and total dose studies of semiconductors [6]. These applications require very low beam currents, ranging from few tens to few thousands of particles per second, corresponding to less than 10^5 times smaller than the usual micro-PIXE intensity (10–100 pA). These conditions impose simultaneously, during long periods of time, a marked reduction in the beam current and precise stability control of the accelerator.

In this work, we present an experimental configuration mounted in the heavy ion microbeam line that allows us to conduct micro-PIXE analysis and quickly change (without modifying the current

delivered by the accelerator) to supplementary studies, like scanning transmission ion microscopy (STIM). In the same way, it allows us to perform SEE experiments on electronic devices and circuits and quickly move to experiments of total dose on them. This setup allows varying and measuring the beam current in a wide range of values from tens of pico- and femto- to atto-amperes without extremely closing the collimators. In the different ranges, it is possible to work with pulsed or quasi-continuous beams, rapidly moving from one condition to another.

Many methods to reduce beam intensity are reported in the literature:

1. Thin gold diffusive foils [7]. In this method, the beam must pass through gold diffusive foils, placed some distance before the object slits, which are usually closed as much as possible. Although this method allows to reduce the current by increasing the emittance of the beam, this procedure can be non-reproducible. That is, the combination of the aperture object slit-diffusion foil thickness does not necessarily lead in each experiment to the same reduction of the current-final spot quality of the microbeam, as this characteristic strongly depends on the quality of the beam provided by the accelerator.
2. Beam attenuators installed in the injection line to adjust the beam intensity without changing the accelerator parameters. A beam attenuator consists of two or three stainless steel meshes. Very low aperture ratios of less than 10^{-4} can be achieved by combining them at each attenuator. By combining attenuators, beam attenuation ratios as low as 10^{-15} can be obtained. The beam energy is usually degraded due to the scattering of the particles at the edges of the mesh's holes [8–11], thereby reducing the quality of the final spot of the microbeam.
3. Very low ion fluxes (10^2 to 10^5 ions/(cm²·s)) are obtained by closing the object and aperture collimators as much as possible to achieve the low beam currents (~1 fA) required for SEE studies in electronics. Beams with high spatial stability are required since even a small displacement of the beam modifies the current on the target [12]. In addition, if the collimators are close enough that the open area is of the same order as the perimeter area, a large amount of dispersed beam is generated at the edges [13]. This scattering produces a wide spatial and energetic distribution of particles around the microbeam axis with different energies and charge states. Eventually, they can pass through the anti-scattering slits and form a halo around the focus. With our system, we solved this problem by switching the beam while remaining the object defining slits closely matching to the normal operating conditions.

In order to obtain low current beams, several facilities reduce the beam current in the accelerator, for example by reducing the ion source output or closing the slits at some point of the accelerator line. The TANDAR accelerator was developed for nuclear research using high energies and high currents of heavy ion beams. The slit stability control used at the output of the bending magnet requires a beam of several nA to obtain a good signal for the feedback loop that controls the terminal voltage. For this reason, the slit control system is not sensitive to low currents beams and it is not suitable for operating the machine under these conditions as it becomes very unstable.

In this way, it is not feasible to inject low enough currents in the microbeam line, to obtain only closing slits, a stable beam with currents of a few tens of ions per second in the microbeam chamber. This is possible in some machine's working condition, although it is very laborious and unstable for long measurement periods and the final current can become unpredictable.

Since we had already developed a beam blanker for micromachining applications, we decided to take advantage of this deflector to vary the current in a fast and simple way. Using this setup, it is unnecessary to close the collimators more than usual for PIXE analysis and the modification of the current in the sample is only achieved by the pulsation of the beam.

In STIM or SEE experiments we close the collimators to normal values and at a given frequency, we put the deflecting system in minimum duty cycle. Under these conditions, we do not have ions on the PIN diode installed in the target chamber. Increasing the duty cycle gradually, we increase the

current of ions that arrive at the target. This is a fast, efficient, and safe procedure because it avoids that a high current of heavy ions reaches the PIN diode and damages it.

2. Materials and Methods

2.1. Pulse Width Modulated Deflection System

The concept behind this method is to use an electrostatic deflector as a beam chopper. A beam chopper is a device that periodically interrupts the particle beam. In our microbeam line, it must travel through the set of aligned object and opening slits separated by a distance of approximately 6 m. Normally, to turn off the beam, a voltage pulse that deflects the beam outside the aperture slits is applied. In this case, the deflector is employed as a “beam blanker”. In the current operation, it is used with the parallel deflecting plates at high potential. That is, the beam is normally off and the pulse beam is generated when it falls into the slit aperture at the bottom of an excitation voltage pulse, annulling the continuous voltage applied to the plates.

With this technique, a continuous particle beam is vertically deflected over the apertures of the slits and, at a given frequency, the average beam current arriving at the device is reduced proportionally to the duty cycle of the deflecting signal. Therefore, if a given frequency has a typical period $f = 1/t$, this period (t) will be made up of two components: the period when the high voltage is applied and the beam suppressed (t_{high}), and the period when the voltage is close to 0 V and the beam is passing up to the sample (t_{low}). Then, the duty cycle is defined as follows:

$$\text{Duty cycle} = \left(\frac{t_{low}}{t_{low} + t_{high}} \right) \times 100\%$$

Two different regimes can be distinguished. If the temporal distance between two consecutive ions is, on average, smaller than t_{low} the resulting beam is going to be composed of bunches. Each bunch is going to be made up of several ions depending on the input current. Section 2.7 shows an application for this mode of operation. In the case that the temporal distance between consecutive ions is greater than t_{low} , a quasi-continuous beam is generated at the input of the aperture slits. This means that each ion is going to be separated from the next for a period larger than t_{high} . The final beam current will depend (on average) on the duty cycle only. However, the regime (continuous or pulsed) will also depend on the frequency.

Physically, the deflector is placed inside the vacuum tube immediately after the object slits. The beam deflector consists of two 15 cm long parallel metal sheets with a 2 mm gap. The conducting layers are made up of thin copper foils laminated onto a non-conductive substrate using epoxy printed circuit board technology. The deflector system is schematically presented in Figure 1.

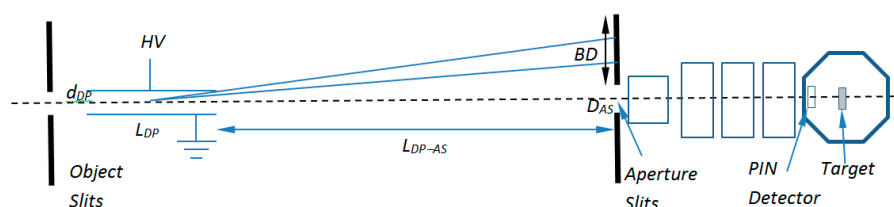


Figure 1. Schematic presentation of high voltage pulses that drive deflector and ion beam path between the object and collimator slits of the microprobe system. L_{DP} = deflector plate length, d_{DP} = deflector gap, L_{DP-AS} = distance of the deflector plates to the aperture slits, BD = beam diameter, D_{AS} = Aperture slits diameter.

For an ion beam of energy E_p and charge q_p , the minimum voltage required across the deflecting plates to ensure that the beam diameter (BD) at the aperture slits is removed completely from the aperture's diameter D_{AS} is given by:

$$V_{DP} = \frac{(D_{AS} + BD)}{2 \cdot L_{DP-AS}} \cdot \frac{E_P}{e \cdot q_P} \cdot \frac{d_{DP}}{L_{DP}}$$

where e is the electron charge and the rest of the symbols are as defined in Figure 1. Therefore, L_{DP} and L_{DP-AS} should be taken as large as possible and d_{DP} as small as possible to minimize the required voltage. In practice, $L_{DP} = 15$ cm and $d_{DP} = 2$ mm were chosen to minimize the capacitance between the plates, and also to achieve a fast switching of the beam. This plate configuration resulted in a capacitance of ≈ 10 pF. In our beamline, the deflector was situated 30 cm after the object slits and 5.8 m before the aperture slits.

As it follows from this formula, the necessary voltage to completely deflect the beam out of the opening slits depends on the beam diameter, which in turn depends on the emittance of the accelerated ion beam, that is, the beam quality repeatability. In each case, there will be a necessary minimum potential ($V_{DP\min}$) to deflect the beam. Usually, in our old accelerator, to reduce the current of the beam, deflection potentials are quickly tested and, to minimize the deflection time, a slightly higher voltage than the necessary minimum is used. For $^{16}\text{O}^{5+}$ beam at 50 MeV energy with $BD = 4.6$ mm diameter at the anti-scattering slits with $D_{AS} = 0.75$ mm a minimum deflection voltage of $V_{DP\min} \approx 70$ V is necessary to blank the beam.

The deflection signal is produced by an arbitrary waveform generator (Rigol®DG4162, Rigol Technologies Inc., Beijing, China). The output signal feeds a high voltage amplifier (Technisches Büro S. Fischer, Ober-Ramstadt, Germany) connected to the electrostatic deflection plates in order to turn on the beam.

2.2. Beam Current Measurement

Simultaneously with the application of the system to change the beam current, one of the most important parameters to consider in any system that is dedicated to the study of radiation damage is the control and measurement of the dose.

The Pelletron charging system of our accelerator causes instability in the beam energy producing fast fluctuations in the current [14], which depends on the stability of the ion source, focusing optics and beam transport, and it may cause slower variations if the operation is not optimal. In order to have an appropriate dose quantification, a precise measurement of the beam current arriving at the sample is required. The most usual method for measuring current for PIXE experiments involves a Faraday cup (FC) placed behind the sample.

State-of-the-art FCs can measure currents as low as 10 fA [15]. For a microbeam of $^{16}\text{O}^{5+}$ with a spot cross-section of a few square microns, 10 fA is equivalent to 10^4 ions/s, which represents a high current for SEE studies. Electronic devices are too thick for the beam to pass through, thus making it necessary to find other ways of dose normalization (online current measurement). Since in SEE studies the current is usually formed by tens or hundreds of ions per second and must be monitored continuously, the use of a FC to measure the current is discarded. Other indirect continuous measurement techniques such as Rutherford backscattering spectrometry (RBS) or X-ray production (PIXE) in the metallic coverage of the devices are only applicable for high-efficiency detectors and larger currents and/or doses.

On the other hand, direct measurement of the particle current as in Scanning transmission ion microscopy (STIM) requires that the samples be completely traversed by the primary ions.

Considering the fact that in SEE studies in electronic components the current cannot be measured continuously, we decided to use a periodical monitoring method, that is, measure several times during the irradiation interrupting the beam without modifying the irradiation conditions. This can be done by placing a particle detector that intercepts the beam path at regular intervals, fast enough to avoid significant dead times between the measurement and the irradiation periods. In each experiment, it is possible to select the periodicity and time of the measurements to obtain an optimum measurement of the particle beam that reaches the sample.

A similar measurement system was described in [16]. In our case, the detector is placed inside the measuring chamber, approximately 10 cm before the sample. Since SEE experiments are usually performed with heavy ion beams with tens of MeV's energy, producing irreversible damage in the semiconductors, it is necessary to use a cheap and easy-to-replace detector as a low-cost alternative to surface barrier detector. As in [16], we decided to use a Hamamatsu S1223-01 Si-PIN photodiode (Hamamatsu, Shizuoka, Japan). This photodiode is widely used as an ion detector and there is extensive literature on its good radiation hardness [17–21]. Thus, the installed setup utilizes a fast electrostatic beam deflector to reduce the current and a movable Si PIN-diode directly measure the beam intensity. This method was used to test SEE produced in a PLL implemented on CMOS 90 nm technology [3].

2.3. Voltage Measurement

To attenuate the beam current, we applied a square signal using different pulse lengths (duty cycles) at a given frequency. This way, one of the plates of the deflector is connected to ground and the other to the variable potential. Thus, ions will reach the sample while the potential lies between 0 and V_{DP} volts. The output pulses $V_{DP}(t)$ of the deflecting plates are shown in Figure 2. $V_{DP} = 70$ V represents the voltage below which a $^{16}\text{O}^{5+}$ beam at 50 MeV starts moving towards the target until it arrives to it. The time intervals indicated at the top of the graph represent the effective enable temporary windows for the shortest pulses allowed by the fast high voltage (HV) amplifier, that is, the times during which the V_{DP} voltage lies below 70 V. The duty cycle in each case will also depend on the pulse frequency.

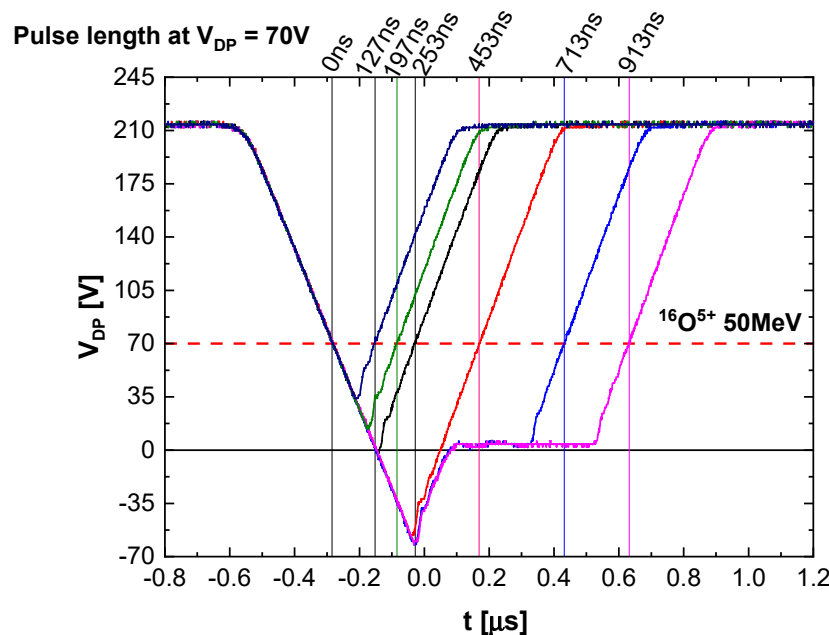


Figure 2. $V_{DP}(t)$ measured at deflecting plates. The effective temporal windows for the shortest pulses allowed by the fast HV amplifier are shown. $V_{DP} = 70$ V represents the necessary minimum voltage to deflect a $^{16}\text{O}^{5+}$ beam.

In Figure 2 the negative overshoots and positive undershoots of the shortest signals are generated by the fast HV amplifier.

The minimum rise time of 220 V deflection pulse provided by the high voltage amplifier is 3.5 ns/V. Assuming a uniform beam of $^{16}\text{O}^{5+}$ at 50 MeV with a current of approximately 3.2 pA, the temporal distance between particles is 0.25 μs . For this beam, according to the calculation above, the temporary enable window V_{DP} occurs between 70 V and 0 V. For a pulse frequency of 1 kHz and an effective duty cycle of 0.025% the temporary enable window between 70 V and 0 V is 253 ns long.

Under these conditions, ion passage is allowed 1000 times/s and the object and collimator slit openings remain unchanged. This makes the operation of low current techniques, such as STIM and IBIC very convenient to use. There are commercial HV switches that can produce high voltage with a few tens of ns rise time. In [22] a beam deflector uses fast high voltage push-pull MOSFET switch (Behlke Electronics GmbH, Kronberg, Germany) having 40 ns rise time for 1 kV pulses. The use of a device with these characteristics would allow us to significantly improve the current reduction range.

2.4. Calibration Process

The setup attenuation range was evaluated at 1 kHz modulating the beam current by varying the duty cycle and measuring the current in the Faraday cup situated in the target chamber. Figure 3 shows the ratio between the beam intensities pulsed-on/pulsed-off as a function of the duty cycle of 220 V deflection pulses at a 1 kHz repetition rate.

The system shows good linearity up to the 0.3% duty cycle when the pulse width is limited by the rise time at 1 kHz (see Figure 2). Below this point, the setup attenuates the beam more than the expected value, but it can still be useful for applications where the linearity is not necessary and reducing the current to the minimum possible is important.

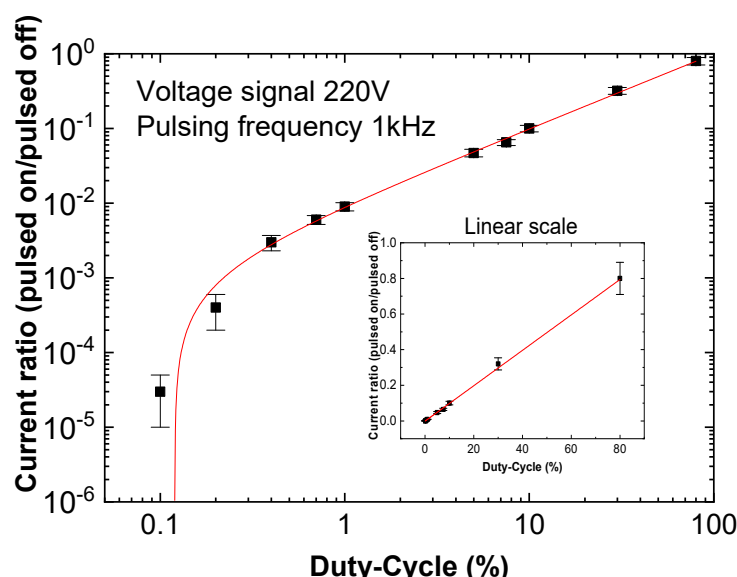


Figure 3. Beam intensity ratios between pulsed-on/pulsed-off conditions as a function of the duty-cycle for a 1 kHz deflection pulse.

2.5. Particle Arrival Statistics

For experiments where a low cumulative dose is desired, it is not necessary to analyze the time distribution of the ions. However, to ensure that SEE happen, it is required that the average time interval between the arrivals of two consecutive ions be much greater than the characteristic response time of the device under study. For MeV ions impinging on electronic components, the pulse duration can range from tens of ps [23] to tens of μ s [24]. However, the main factor limiting the number of pulses that can be recorded is usually the number of waveforms per unit of time that the oscilloscope used for the SEE detection can process. This number of waveforms can be in the order of a few thousands per second or less.

Accordingly, we measured the number of ions in 1 ms intervals during one minute with a MultiChannel Scaler (Ametek, Oak Ridge, TN, USA) and a silicon PIN diode as a detector. The particle beam intensity without deflection was \approx 22,000 ions/s and the deflector was configured using a 0.1% duty cycle and 100 Hz frequency.

In order to study the arrival time distribution, we made a histogram showing the time between two consecutive ions hitting the target. As it is shown in Figure 4, the resulting histogram can be

approximated by an exponential decay function with a mean time of 45 ms. It is well known that Poisson processes show this kind of distribution when the time between events is analyzed. As a result, we can assume that the process is random and the mean time is consistent with the expected value (for a quasi-continuous beam). If the beam were pulsed instead of quasi-continuous, a large number of events should be observed on the first time interval.

In order to measure the beam current when a thick sample is placed on the target, we designed a movable detector that is periodically placed in front of the beam, inside the vacuum chamber. The interposition of the detector is performed by using a servo-motor handled by an Arduino microcontroller based system. This system measures the number of incident ions at regular intervals with a transit time (dead time) of about 60 ms/measurement. To verify that the measured current with this method is representative of the number of ions impinging on the target, another PIN diode was placed as target and the counting for both detectors was recorded. The servo-motor was programmed to enable the beam transmission at intervals of 1 s. Figure 5 shows the measured current on the servo PIN-diode. Inverted peaks correspond to time intervals where the servo PIN-diode is out of the beam. The circles represent the counting rate of the target PIN-diode.

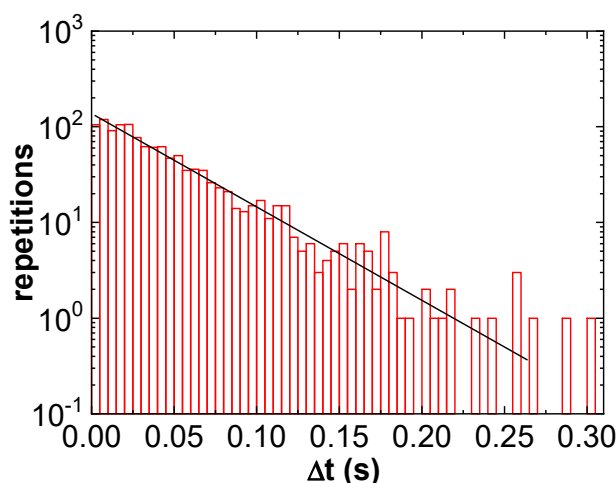


Figure 4. Histogram of the time between two arrivals. The linear tendency in a logarithmic scale plot shows an exponential relation, typical in Poisson distributions.

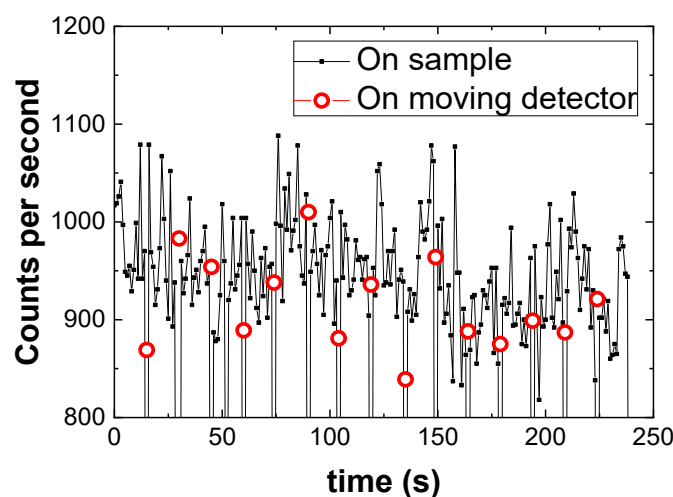


Figure 5. Servo PIN-diode and target PIN-diode counting rate. The current fluctuations are originated by the terminal voltage fluctuations due to the chain charging system of the accelerator.

Figure 6 shows the histogram of the counting rate at the target PIN-diode. The width of the distribution (about 10%) is principally given by fluctuations of the beam current, and it is the principal source of uncertainty in dose determination. For this particular beam conditions (about 10^3 ions/s), the difference between the averages counting rates measured on the mobile PIN-diode and on the target PIN-diode is about 0.35σ . The maximum current that can be achieved with this technique is limited by the time response of the detector and amplifier system which is in the order of 10^3 ions per second for most of the solid-state ion detectors (besides the damage caused by heavy ions with tens of MeVs energy). With this technique, we can obtain total accumulated ions in the range of 10^3 ions for a low current and short time irradiation up to 3.6×10^6 ions for a one-hour long irradiation with a relative uncertainty of $\approx 10\%$ covering an area of $10 \mu\text{m}^2$ to $10^6 \mu\text{m}^2$.

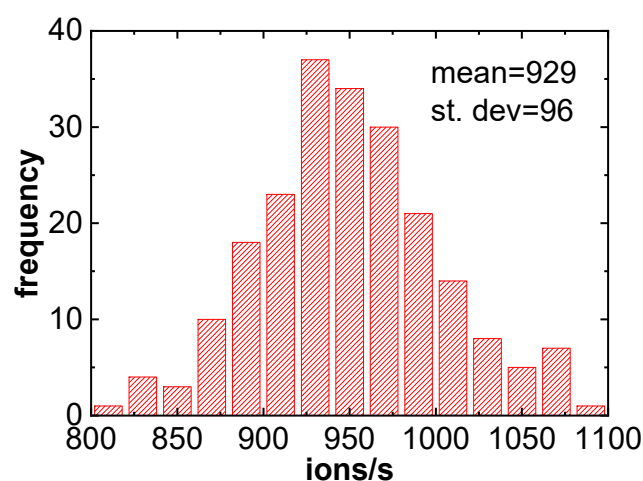


Figure 6. Histogram of the counting rate at the sample PIN-diode in a 250 s measurement run.

2.6. Low Current Application: SEE in a CMOS Output Buffer

As an example for SEE measurements with the previously described system, two digital output buffers ($0.5 \mu\text{m}$ CMOS (Complementary Metal-Oxide Semiconductor) process) were tested. As shown in Figure 7 the device was formed by cascading four CMOS inverters with increasing sizes from input to output. This kind of circuit is used to increase the driving capability of a logic gate made by minimum size transistors for large load capacities, so it is present in the output of most digital integrated circuits (ICs). Each inverter is composed of one PMOS (p-type MOS) and one NMOS (n-type MOS) so, under normal conditions, only one of the transistors is ON (saturation) while the complementary is OFF (cut-off).

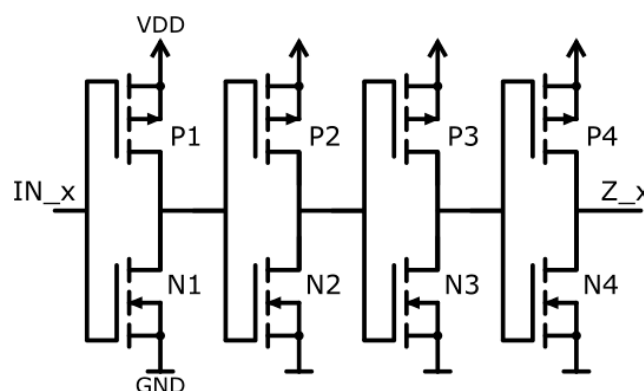


Figure 7. Output buffer schematic.

To test both operation states (high state follower and low state follower), each buffer had its input fixed to one of the logic levels: BUFFER 0 had its input fixed at ground potential (P1/N2/P3/N4 in the ON state) while BUFFER 3 had its input at VDD (drain to drain voltage) (5 V) potential (N1/P2/N3/P4 in the ON state).

A 3 μm beam spot of $^{32}\text{S}^{8+}$ at 75 MeV was used for the experiment. The IC was mounted on a printed circuit board inside the high vacuum microbeam chamber. The outputs of both buffers were connected outside the chamber through BNC connectors and acquired by a 1.5 GHz bandwidth and 20 GS/s oscilloscope (Teledyne Lecroy WavePro 715Zi, Teledyne Lecroy, Chesnut Ridge, NY, USA) with the trigger level slightly above the noise. The input signal of the XY deflector coils amplifier was acquired in two channels of the oscilloscope. Two different transients are shown in Figure 8.

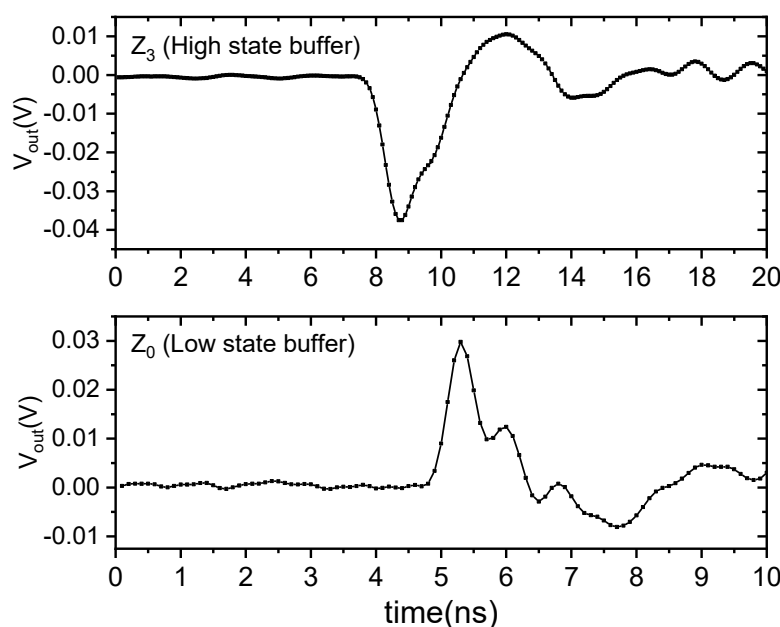


Figure 8. Typical SEE transient responses for each buffer (AC coupled signals). The negative output pulse corresponds to BUFFER 3 and the positive to BUFFER 0. The reflections are the result of the slight mismatching connections impedances.

As expected, the measured output pulses were negative for BUFFER 3 (High state follower) and positive for BUFFER 0 (Low state follower).

Figure 9 shows the X-Y map of event triggers overlapped with the actual layout of the tested buffers. The SEE coordinates were over the transistors N1/P2/N3/P4 of BUFFER 3 and over P1/N2/P3/N4 of BUFFER 0. All of these devices are the ones that were in cut off operation mode.

2.7. Radiation Damage in LiNbO_3 Applying the Constant Gradient Technique

In order to show the potential of using the electrostatic deflector on demand as beam current controller, it was used in combination with the microbeam scanning system with the purpose of generating a smooth damage gradient with different applied doses on a piece of LiNbO_3 x-cut. Previous studies [1] show that using fluences of 5×10^{12} ions/ cm^2 of Cl^{35} at 70 MeV generate lattice damage in a way that the etching rate in an HF (50%) acid increases drastically. We used a similar projectile as in [4,5], a 5 μm beam spot of $^{32}\text{S}^{8+}$ at 75 MeV energy and $250 \times 250 \mu\text{m}^2$ scanned area. The electrostatic deflector was used to reduce the flux using a pulse width modulation (PWM) signal phased with a triangular (sawtooth) signal.

The used waveform generator allows to produce signals of up to 16,384 points. We divided the data string into 128 segments of 128 points each. Every segment was set up in order to have a duty cycle of $\approx 0.78\%$ larger than the previous one. In the second channel, a constant voltage that increases

every 128 points (stepped waveform) was configured (Figure 10). That signal was connected to one of the inputs of the scanning amplifier corresponding to the X-axis. The Y-axis input was connected to another triangle wave generator, which scans the beam along the Y-axis during the 128 steps intervals for the different X positions. The frequencies were 256 Hz for the X-axis and 2 Hz for the Y-axis. The fluence was controlled measuring the X-rays emitted by the sample during the irradiation (Figure 11). We had previously normalized the X-ray production of the sample with the ion current. At the end of the experiment, the fluence was linearly decreasing from 8.08×10^{13} to 6.31×10^{11} ions/cm² in 128 steps.

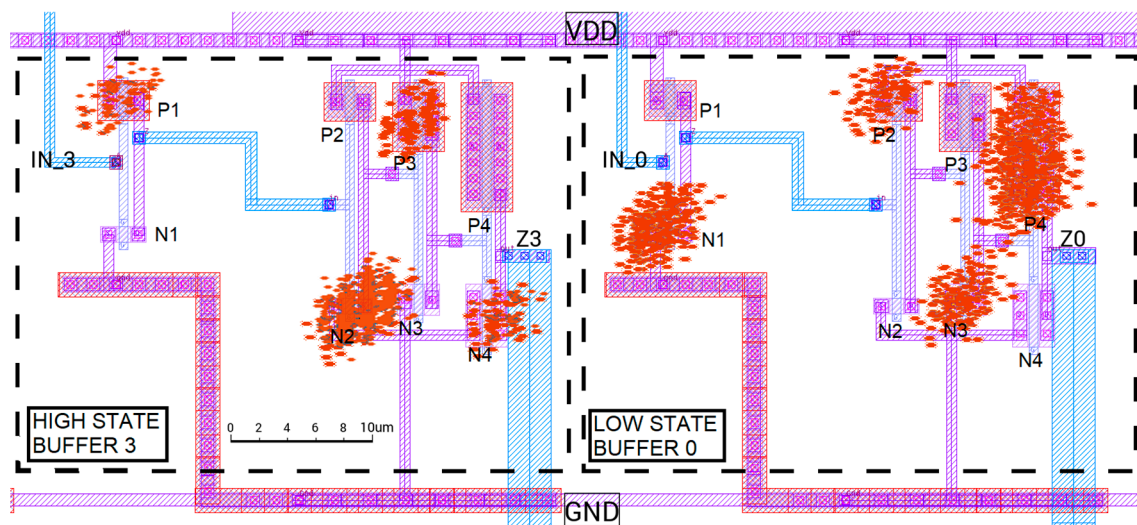


Figure 9. Map of all SEE triggering coordinates overlaid with the layout of both tested buffers. Events were only detected on devices in cut off operation mode.

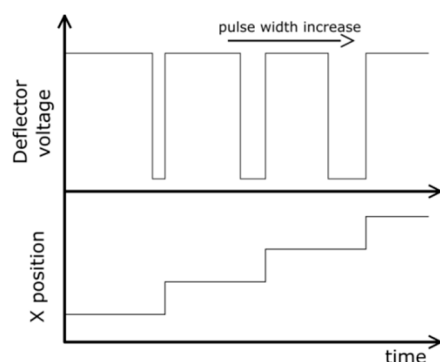


Figure 10. Schematic figure showing the phased signals of position and deflection voltage used for constant gradient dose experiment.

Furthermore, in order to characterize the damage in the material, micro-Raman technique was used. The spectra were recorded using a LabRAM HR Raman system (Horiba Jobin Yvon, Kyoto, Japan), equipped with two monochromator gratings and a charge-coupled device detector. An 1800 g/mm grating and a 100 μm hole results in a spectral resolution of 1.5 cm^{-1} . Polarized light of the 514.5 nm Ar laser line was used as the excitation source. Measurements were taken in backscattering geometry, with a 50 \times magnification under a confocal microscope coupled to the spectrograph. Under these conditions, the spatial resolution of the system is about 5 μm . In this range, the irradiated zone can be easily distinguished using conventional microscopy due to the changes in the optical properties of the material. The spectra were taken from the edge of the irradiated zone up to 280 μm further. The 368 cm^{-1} peak area was used to normalize the spectra because it showed slight or no change at different sample positions.

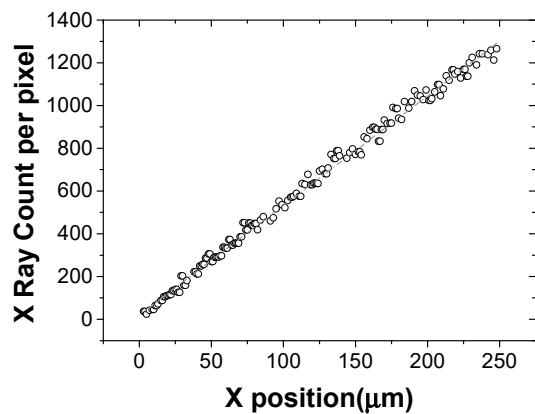


Figure 11. X-ray production vs. X position. Each point represents X-ray counts averaged along the Y-axis at each X position.

As it can be seen in Figure 12, as the doses increases, peaks present in the unirradiated horizontal polarization ($Y(XX)Y$) gradually appear in the irradiated vertical polarization ($Y(XZ)Y$), and vice versa. In order to analyze this behavior, the sample was metalized with 40 nm gold and the irradiated zone was measured using an optical profilometer. As shown in Figure 13 there is a gradual increment of the sample thickness caused by the accumulated dose (swelling).

LiNbO_3 presents photo-elastic properties [25] so mechanical stress can induce a shift in the polarization angle of the light that passes through the crystal. Probably, irradiation is introducing mechanical stress in the crystal. This effect may be the reason why Raman peaks present on each polarization are gradually appearing on the other, as irradiation dose increases.

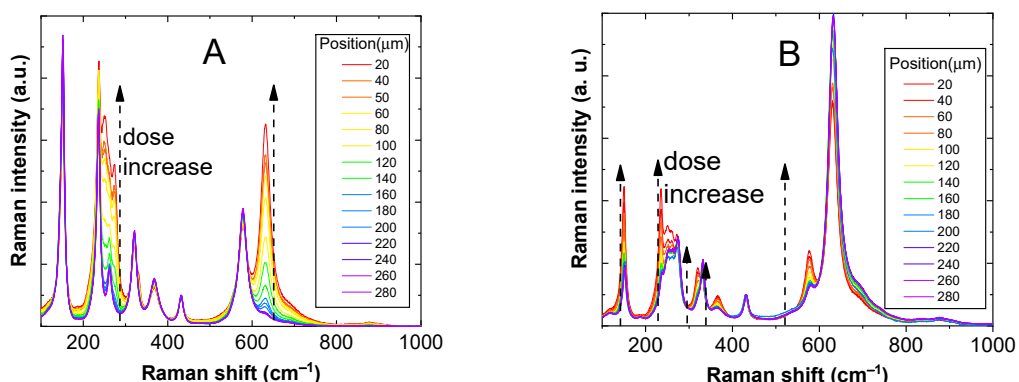


Figure 12. Micro-Raman spectra vertically (A) and horizontally (B) polarized. The laser beam was placed at different points in the irradiated area in order to show the effects of different doses.

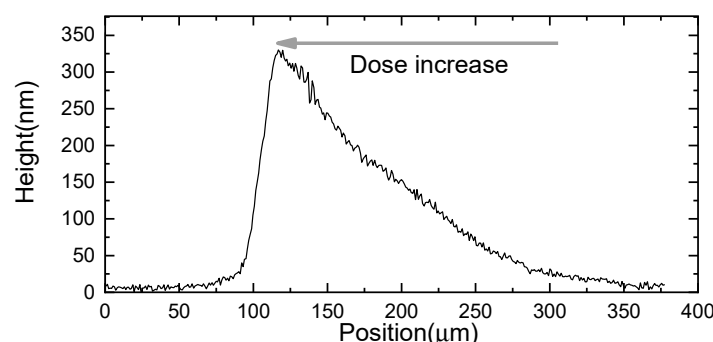


Figure 13. X-profile of the irradiated zone measured with an optical profilometer.

Although it is not the purpose of this paper to explain the causes of these changes, it is clear that this technique allows characterizing the evolution of damage in a given material for many different doses making a single irradiation.

3. Conclusions

We present a system that allows to modify a heavy ion current in a fast, simple and completely electronically controlled way, based on an electrostatic deflector.

We achieved attenuation ratios up to 10^{-4} and below for a frequency of 1 kHz. Lower ratios may be achieved using faster amplifiers and/or lower frequencies. The method has been characterized in linearity and time domain statistics. If the intensity of a uniform beam is such that the temporal distance between particles is of the same order or lower than the minimum deflecting pulse width, the particle arrival can be described as a Poisson process. We also presented a low-cost method to measure online beam currents in the order of a few tens of particles per second. As an example for SEE measurements using the previously described system, two 0.5 μm technology CMOS digital output buffers were tested using a 3 μm beam spot of $^{32}\text{S}^{8+}$ at 75 MeV bombarding energy. The use of a heavy ion microbeam allows evaluation of the behavior of the circuit under the working conditions expected for a device performing in space applications. Captured ASET (analog single event transient) were mapped on the circuit layout and assigned to individual transistors on the circuit. On the other hand, the versatility of the fast regulation current system was proved through the application of a novel constant irradiation gradient technique, which was used to study the evolution of the radiation effects in a mono-crystal of LiNbO_3 by micro-Raman analysis. This method allowed the generation of a damage pattern with fluences linearly decreasing from 8.08×10^{13} to 6.31×10^{11} ions/ cm^2 in 128 steps. It can also be used to study the dose required for micromachining of different materials using proton or heavy ion beam writing.

Author Contributions: Conceptualization, methodology, and validation: N.A.V.; investigation and resources: N.A.V., M.E.D., N.A.M., E.d.I.F., and E.B.H.; writing: N.A.V., E.B.H. and M.E.D.; supervision: M.E.D.

Funding: This work has been funded by MINCyT under contract PICT 1210/2013.

Conflicts of Interest: The authors declare no conflict of interest.

References

1. Stolar, P.; Kreiner, A.J.; Debray, M.E.; Caraballo, M.E.; Valda, A.A.; Davidson, J.; Davidson, M.; Kesque, J.M.; Somacal, H.; DiPaolo, H.; et al. Microdistributions of Prospective BNCT-Compound CuTCPH in Tissue Sections with a Heavy Ion Microbeam. *Appl. Radiat. Isot.* **2004**, *61*, 771–774. [[CrossRef](#)]
2. Muscio, J.; Somacal, H.; Burlon, A.A.; Debray, M.E.; Kreiner, A.J.; Kesque, J.M.; Minsky, D.M.; Valda, A.A.; Davidson, M.; Davidson, J.; et al. Radiographic Technique for Densitometric Studies Using Heavy Ion Microbeams. *AIP Conf. Proc.* **2007**, *947*, 491–492. [[CrossRef](#)]
3. Günther, M.; Debray, M.; Corti, H. Preliminary Results of the Degradation of Platinum Based Catalyst in PEM Fuel Cells Using PIXE. In *Role of Nuclear Based Techniques in Development and Characterization of Materials for Hydrogen Storage and Fuel Cells*; IAEA: Vienna, Austria, 2012; pp. 99–106.
4. Nesprías, F.; Debray, M.E.; Davidson, J.; Kreiner, A.J.; Vega, N.; De La Fournière, E. Millimeter Length Micromachining Using a Heavy Ion Nuclear Microprobe with Standard Magnetic Scanning. *Nucl. Instrum. Methods Phys. Res. Sect. B Beam Interact. Mater. At.* **2013**, *300*, 68–73. [[CrossRef](#)]
5. Nesprías, F.; Venturino, M.; Debray, M.E.; Davidson, J.; Davidson, M.; Kreiner, A.J.; Minsky, D.; Fischer, M.; Lamagna, A. Heavy Ion Beam Micromachining on LiNbO_3 . *Nucl. Instrum. Methods Phys. Res. Sect. B Beam Interact. Mater. At.* **2009**, *267*, 69–73. [[CrossRef](#)]
6. Sondon, S.; Falcon, A.; Mandolesi, P.; Julian, P.; Vega, N.; Nesprías, F.; Davidson, J.; Palumbo, F.; Debray, M. Diagnose of Radiation Induced Single Event Effects in a PLL Using a Heavy Ion Microbeam. In Proceedings of the 2013 14th Latin American Test Workshop-LATW, Cordoba, Argentina, 3–5 April 2013; pp. 3–7. [[CrossRef](#)]

7. Cervellera, F.; Donolato, C.; Egeni, G.P.; Fortuna, G.; Nipoti, R.; Polesello, P.; Rossi, P.; Rudello, V.; Vittone, E.; Viviani, M. The Legnaro Ion Microprobe in Low Current Experiments. *Nucl. Instrum. Methods Phys. Res. Sect. B Beam Interact. Mater. At.* **1997**, *130*, 25–30. [[CrossRef](#)]
8. Hirao, T.; Nishiyama, I.; Kamiya, T.; Nishijima, T. Effects of Micro-Beam Induced Damage on Single-Event Current Measurements. *Nucl. Instrum. Methods Phys. Res. Sect. B Beam Interact. Mater. At.* **1995**, *104*, 508–514. [[CrossRef](#)]
9. Hirao, T.; Mori, H.; Laird, J.S.; Onoda, S.; Wakasa, T.; Abe, H.; Itoh, H. Studies on Single-Event Phenomena Using the Heavy-Ion Microbeam at JAERI. *Nucl. Instrum. Methods Phys. Res. Sect. B Beam Interact. Mater. At.* **2003**, *210*, 227–231. [[CrossRef](#)]
10. Sexton, F.W.; Horn, K.M.; Doyle, B.L.; Shaneyfelt, M.R.; Meisenheimer, T.L. Effects of Ion Damage on IBICC and SEU Imaging. *IEEE Trans. Nucl. Sci.* **1995**, *42*, 1940–1947. [[CrossRef](#)]
11. Arakawa, K.; Nakamura, Y.; Yokota, W.; Nara, T.; Agematsu, T.; Okumura, S.; Ishibori, I.; Fukuda, M. Status Report on JAERI-AVF Cyclotron. In Proceedings of the 14th International Conference on Cyclotrons and their Applications, Cape Town, South Africa, 8–13 October 1995; p. B06.
12. Silvestrin, L. Characterization of Electronic Circuits with the SIRAD IEEM: Developments and First Results. Ph.D. Thesis, Università Degli Studi di Padova, Padova, Italy, 2011. Available online: http://paduaresearch.cab.unipd.it/4024/1/Thesis_PhD_Silvestrin.pdf (accessed on 3 March 2019).
13. Nobiling, R.; Civelekoglu, Y.; Povh, B.; Schwalm, D.; Traxel, K. Collimation of Ion Beams to Micrometer Dimensions. *Nucl. Instrum. Methods* **1975**, *130*, 325–334. [[CrossRef](#)]
14. Fauska, H.; Heagney, J.S.; Mofgan, T.J.; Schmidt, F.H. Terminal Voltage Fluctuations of a Van der Graaf Accelerator. *IEEE Trans. Nucl. Sci.* **1967**, *14*, 166–168. [[CrossRef](#)]
15. Hypolite, B.P.; Evariste, W.T.; Adolphe, M.I.; Kemgang, K. An Accurate Low Current Measurement Circuit for High-Resolution Energy Spectroscopy Systems An Accurate Low Current Measurement Circuit for High-Resolution Energy Spectroscopy Systems. *Asian J. Appl. Sci.* **2015**, *3*, 952–957.
16. Stoytschew, V.; Bogdanović Radović, I.; Demarche, J.; Matjačić, L.; Siketić, Z.; Webb, R. MeV-SIMS Yield Measurements Using a Si-PIN Diode as a Primary Ion Current Counter. *Nucl. Instrum. Methods Phys. Res. Sect. B Beam Interact. Mater. At.* **2016**, *371*, 194–198. [[CrossRef](#)]
17. Simon, A.; Kalinka, G.; Jakšić, M.; Pastuović, Ž.; Novák, M.; Kiss, Á.Z. Investigation of Radiation Damage in a Si PIN Photodiode for Particle Detection. *Nucl. Instrum. Methods Phys. Res. Sect. B Beam Interact. Mater. At.* **2007**, *260*, 304–308. [[CrossRef](#)]
18. Simon, A.; Kalinka, G. Investigation of Charge Collection in a Silicon PIN Photodiode. *Nucl. Instrum. Methods Phys. Res. Sect. B Beam Interact. Mater. At.* **2005**, *231*, 507–512. [[CrossRef](#)]
19. Ramírez-Jiménez, F.J.; Aguilera, E.F.; López-Callejas, R.; Benítez-Read, J.S.; Pacheco-Sotelo, J. A Novel Application of a PIN Diode-Preamplifier Set for the Measurement of Charged Particles. *Nucl. Instrum. Methods Phys. Res. Sect. A Accel. Spectrometers Detect. Assoc. Equip.* **2005**, *545*, 721–726. [[CrossRef](#)]
20. Ramírez-Jiménez, F.J.; Mondragón-Contreras, L.; Cruz-Estrada, P. Application of PIN Diodes in Physics Research. *AIP Conf. Proc.* **2006**, *857*, 395–406. [[CrossRef](#)]
21. Devès, G.; Matsuyama, S.; Barbotteau, Y.; Ishii, K.; Ortega, R. Characterization of Si P-i-n Diode for Scanning Transmission Ion Microanalysis of Biological Samples. *Rev. Sci. Instrum.* **2006**, *77*, 056102. [[CrossRef](#)]
22. Jakšić, M.; Medunić, Z.; Skukan, N. On the Use of Pulsed Microbeam in IBIC. *Nucl. Instrum. Methods Phys. Res. Sect. B Beam Interact. Mater. At.* **2003**, *210*, 176–180. [[CrossRef](#)]
23. Rostewitz, M.; Hirche, K.; Latti, J.; Jutzi, E. Single Event Effect Analysis on DC and RF Operated AlGaN/GaN HEMTs. *IEEE Trans. Nucl. Sci.* **2013**, *60*, 2525–2529. [[CrossRef](#)]
24. Buchner, S.; McMorrow, D.; Poivey, C.; Howard, J.; Boughassoul, Y.; Massengill, L.; Pease, R.; Savage, M. Comparison of Single-Event Transients Induced in-an Operational Amplifier LM124. by Pulsed Laser Light and a Broad Beam of Heavy Ions. *IEEE Trans. Nucl. Sci.* **2004**, *51*, 2776–2781. [[CrossRef](#)]
25. Weis, R.S.; Gaylord, T.K. Lithium Niobate: Summary of Physical Properties and Crystal Structure. *Appl. Phys. A Solids Surf.* **1985**, *37*, 191–203. [[CrossRef](#)]

